PRE-BREAKDOWN LASER TARGET VAPORIZATION AND ENHANCED THERMAL COUPLING

Dennis A. Reilly, et al

Avco Everett Research Laboratory, Incorporated

Prepared for:

Office of Naval Research
Advanced Research Projects Agency

August 1974

PRE-BREAKDOWN LASER TARGET VAPORIZATION AND ENHANCED THERMAL COUPLING

FINAL TECHNICAL REPORT

by

Dennis A. Reilly and Peter S. Rostler

AVCO EVERETT RESEARCH LABORATORY, INC.
a Subsidiary of Avco Corporation
Everett, Massachusetts

Contract No. N00014-73-C-0457

August 1974

supported by

ADVANCED RESEARCH PROJECTS AGENCY
DEPARTMENT OF DEFENSE

and

monitored by

OFFICE OF NAVAL RESEARCH
DEPARTMENT OF THE NAVY
Arlington, Virginia

FOREWORD

ARPA Order Number - 2439

Program Code Number - 3E20

Name of Contractor - Avco Everett Research Laboratory, Inc.

Effective Date of Contract - 15 June 1973

Contract Expiration Date - 28 February 1974

Amount of Contract - $146,985

Contract Number - N00014-73-C-0457

Principal Investigator and Phone Number - Dennis A. Reilly, (617) 389-3000, ext. 426

Scientific Officer - Director, Naval Research Laboratory, 4555 Overlook Ave., S.W., Washington, D.C.

Short Title of Work - Pre-Breakdown Laser Target Vaporization and Enhanced Thermal Coupling

ABSTRACT

Vaporization of metallic targets under the influence of pulsed CO_2 laser radiation is observed prior to breakdown plasma formation using the techniques of atomic absorption spectroscopy and time resolved emission spectroscopy. Aluminum targets vaporize in times short compared to predictions based on bulk thermal properties, a behavior which may be attributable to microsurface imperfections. Plasma formation times are consistent with models that assume the presence of metallic vapor.

Aluminum targets that experienced plasma breakdown exhibited cratering vs little visible surface damage to targets irradiated at fluxes just below the breakdown threshold. Thermal energy deposition per unit incident energy was increased by a factor of three when the breakdown threshold was exceeded.

TABLE OF CONTENTS

LIST OF ILLUSTRATIONS

I. INTRODUCTION

Laser supported absorption waves are a well documented phenomenon in which a laser beam's energy is partially or fully absorbed in a front of ionized gas which is maintained by the absorption process. These waves fall into two broad categories. Laser supported detonation (LSD) waves are characterized by absorption lengths less than the laser beam diameter, pressures considerably greater than ambient pressure, and supersonic velocities. Laser supported combustion waves (LSC) attenuate the beam's energy over a distance on the order of or greater than the beam diameter, the pressure is on the order of ambient and the velocities are less than sonic.

It is also well documented both theoretically[1] and experimentally[2] that breakdown, i.e., the creation of substantial ionization, in clean air at STP requires laser fluxes of greater than 2×10^9 watts/cm^2 for 10.6 μ wavelength radiation. Under such intensities a detonation wave results. However, it has been observed that breakdown and subsequent wave propagation can occur at substantially lower fluxes if the beam impinges on a target consisting of any one of a broad range of materials.

The ignition of absorption waves can have a number of important implications with regard to laser applications. It is clear that a highly ionized absorption wave that propagates a sufficient distance away from a target will shield the target from further absorption of radiation. If the wave is in detonation regime, the high pressure volume recedes from the target leading to a decrease in the impulsive coupling.

On the other hand, there is experimental evidence indicating that a target with small absorptivity to the incoming radiation can experience enhanced thermal coupling if an absorption wave is ignited.[3] Possible explanations for this effect are re-radiation by the highly absorbing plasma back to the target and/or convective, conductive transfer of heat to the target. There are also theoretical predictions that a detonation wave which is allowed to propagate no further than one laser beam diameter away from the target can efficiently couple impulses to the target.[4]

Since target effects can be dramatically dependent on the presence or non-presence of a laser supported absorption wave, it is important to know under what conditions - target material, surface temperature and roughness; ambient gas pressure and flow; laser flux, pulse time and spot size - these waves are ignited. A fair body of empirical data already exists. However, lacking a suitably tested model for the mechanism responsible for the ignition of these waves, the present data has not been correlated nor is it possible to extrapolate to conditions beyond those tested. This latter point is particularly important if one is to project possible countermeasures either offensive or defensive.

It is the purpose of the present investigation to determine the mechanism of wave ignition under a limited set of conditions which are of interest to future applications of pulsed laser devices. Specifically, this investigation will deal with fluxes in the range of 10^6 to a few times 10^7 watts/cm^2 at the largest spot sizes consistent with the 10^6 watt 10.6 μ laser output. Most of the work will deal with metallic targets.

II. BREAKDOWN INITIATION STUDIES

Three principal mechanisms have been proposed to explain surface plasma breakdown. At high incident flux values (> 10^8 watts/cm^2) the electric field associated with the wave would be sufficient to induce field emission from needle shaped points on the material surface. Electrons would gain sufficient energy from the field within their mean free path to ionize an air molecule. A cascade process follows leading to full ionization.[5] A similar model, at somewhat lower fluxes, derives the initial electrons from thermionic emission. However, it seems likely that points hot enough to emit thermionically would soon vaporize. Not only would this remove the emitting points, but the resulting vapor would dominate the subsequent physics.

At fluxes of 10^6 to 10^8 watts/cm^2 most theoretical investigations[5, 6] have assumed that the target first vaporizes and that the initial electron concentration, derivable from the Saha equation evaluated at the vaporization temperature, then increases due to a cascade ionization process in the target vapor.

Although these models are reasonably successful in predicting cascade ionization times in the vapor which are consistent with observed breakdown times, they all must call for anomalous target absorptivities or thermal conductivities in order to generate target vapor on time scales consistent with observed breakdown times. For instance, an Al surface is expected to vaporize in 27 μsec with an absorbed flux of 10^6 watts per cm^2.

However, the initial absorptivity is ≈ 3% which implies 27 μsec for incident fluxes of 3×10^7 watts/cm^2. Breakdown is observed on a time scale of μsecs at this flux.

One explanation for rapid vaporization would be heating of small flakes or points on the surface which are in poor thermal contact with the bulk material. The fact, observed in our studies as well as others, that a surface that does not break down at a given flux can be induced to do so by roughening it with emery cloth gives substance to this view.

One of the principal objectives of this investigation was to determine if target vapor actually evolves from the target previous to breakdown, regardless of the surface microstructural details that lead to the vaporization. Detection of the vapor would greatly enhance the credence one could place on the theoretical models that assume vaporization.

Since the required vapor for breakdown can be quite minute and since the vapor need not be strongly optically emitting at its vaporization temperature, a particularly sensitive technique is needed to detect its presence. To this end we have employed a modification of the method of Resonance Absorption Spectroscopy[7] which has long been used by chemists for detecting trace elements.

A. ATOMIC ABSORPTION SPECTROSCOPY

1. Theoretical Background

The absorption coefficient for photons with a frequency corresponding to the energy difference between two atomic states is given by the expression

$$\alpha = N \frac{\pi c r_e f}{\Delta \nu}$$

where α is the absorption coefficient in inverse cm, N is the number density of atoms in the lower state of the transition, r_e is the classical electron radius, c is the speed of light and f is the oscillator strength for the transition involved. The width of the transition, $\Delta\nu$ in frequency units is governed by a number of considerations. At low densities in a cold gas, $\Delta\nu$ is the natural line width which is given by the inverse of the lifetime of the transition. In the limit of high density, resonance broadening, in which excitation from an excited atom is transferred to an unexcited atom of the same species, dominates and the frequency width is given by[8]

$$\Delta\nu = \frac{3}{2} \frac{r_e c^2}{\nu} Nf \left(\frac{g_\ell}{g_u}\right)^{1/2}$$

where g_ℓ and g_u are the multiplicities of the lower and upper states respectively. The absorption coefficient in this case is

$$\alpha = \frac{2}{3} \pi \left(\frac{g_u}{g_\ell}\right)^{1/2} \frac{1}{\lambda}$$

that is, the radiation is absorbed over a distance on the order of a wavelength, λ, independent of the density or the f number. This condition of high density could be expected immediately above the surface of a strongly vaporizing target.

The most generally expected broadening mechanism over the range of experimental conditions would be due to the thermal motions of the hot vapor giving a Doppler width of

$$\Delta\nu = \sqrt{2\pi k T_a / M_a}\ \nu/c$$

where T_a and M_a are respectively the temperature and atomic mass of species a. This mechanism is dominant for densities satisfying

$$N \ll 10^{16} \sqrt{\frac{\Theta_a / A_a}{\lambda_\mu^2 f}} \left(\frac{g_u}{g\ell}\right)^{1/2}$$

where Θ_a is the vapor temperature in eV, A_a is the atomic mass number and λ_μ is the wavelength of the transition in μ.

As a numerical example, we consider aluminum vapor at the vaporization temperature of 2750°K and a ground state population of $N = 3.6 \times 10^{11}/cm^3$. Virtually all the electrons will be in the ground state so N also represents the total atomic density. Choosing for example the aluminum resonance transition at $\lambda = 3092$ Å with an f number of 0.79, we find that Doppler broadening is dominant and the absorption coefficient is 1/cm. This number illustrates the extreme sensitivity of the method to trace quantities of target vapor.

2. Experimental Method

The basic experimental plan has two configurations. An appropriate source of resonance radiation light for the desired target vapor transition is either directed across the target, as shown in Fig. 1, or else is aimed to shine on the same target spot as the impinging CO_2 laser radiation, as shown in Fig. 2. The light passing by the target or reflecting from it is collected with a lens and directed to a Jarrell Ash 0.25 meter monochrometer which serves to filter out undesired lines from the resonance radiation source and to partially block light due to a developing target breakdown. The transmitted radiation is detected with a 1P28 photomultiplier.

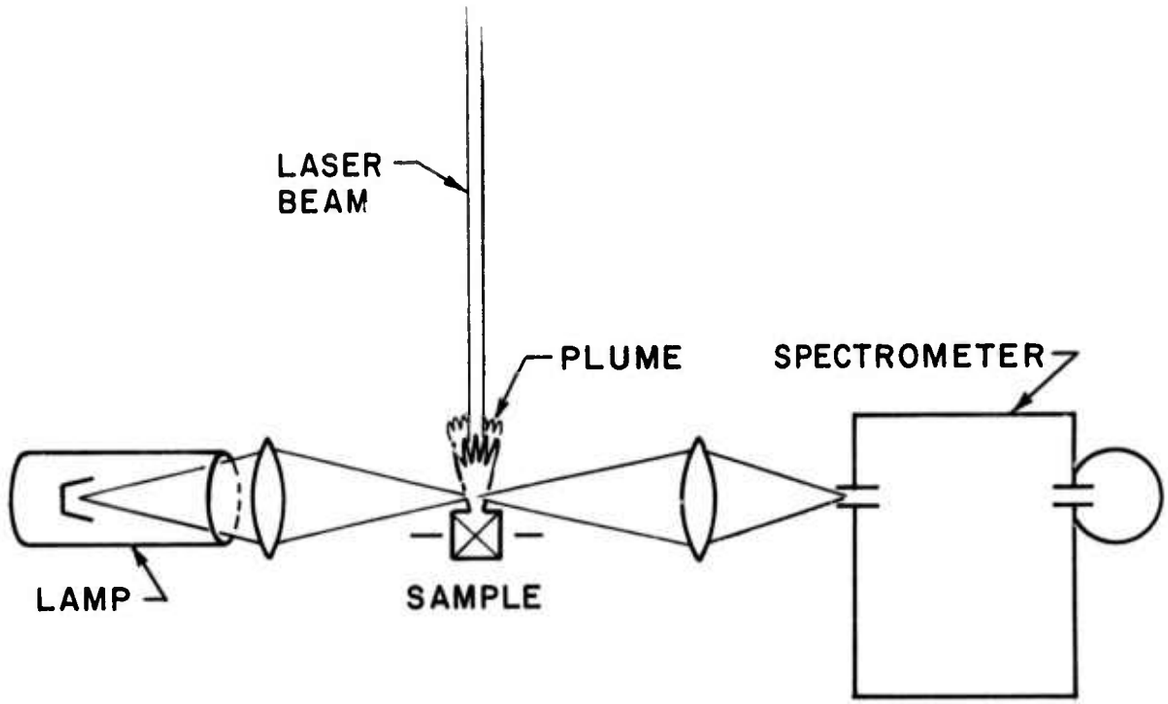

Fig. 1 Schematic of Experimental Apparatus

ATOMIC ABSORPTION SPECTROSCOPY
(REFLECTED LIGHT)

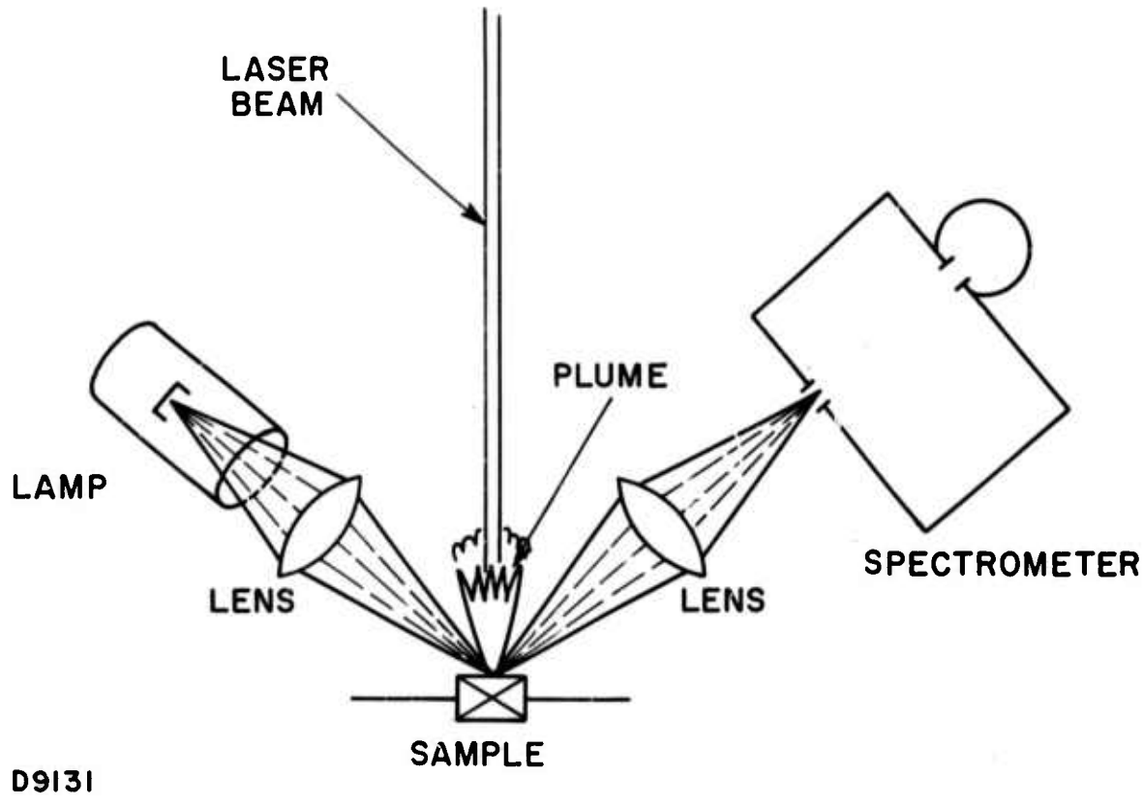

Fig. 2 Schematic of Experimental Apparatus

In the first configuration, the spatial resolution (measured experimentally by observing the intensity of transmitted light as a function of distance as a sharp edged blade is moved across the focal spot near the target) is ~1 mm as shown in Fig. 3. This leads to some ambiguity in the density of the target vapor since partial transmittal of light could be due to very dense completely absorbing vapor that has moved only part way across the resolution element. On the other hand, this configuration has the advantage that the probe beam can be positioned at various distances from the target allowing the velocity of the vapor to be obtained by noting time of onset of probe beam absorption. This information can in turn be used to offset the aforementioned ambiguity.

If a target were to vaporize uniformly, all the probe light in the second configuration would intercept the vapor as soon as it left the target. However, this method suffers several disadvantages. Firstly, changes in the target reflectivity or scattering coefficient, certainly expected in the case of prevaporization melt, would lead to changes in the received signal. Secondly, the vapor has a velocity component in the direction of the probe beam which shifts the center of the absorption line away from the center of the probe line radiation. For these reasons, only limited data were taken by this method and they will not be discussed here.

The resonant radiation employed in these experiments was obtained from standard hollow cathode lamps manufactured by Perkin Elmer Corp. for use in flame spectroscopy apparatus. Different lamps were obtained with cathodes constructed of the same material as the test target material under investigation. These materials included Zn, Al and Ti. The lamps

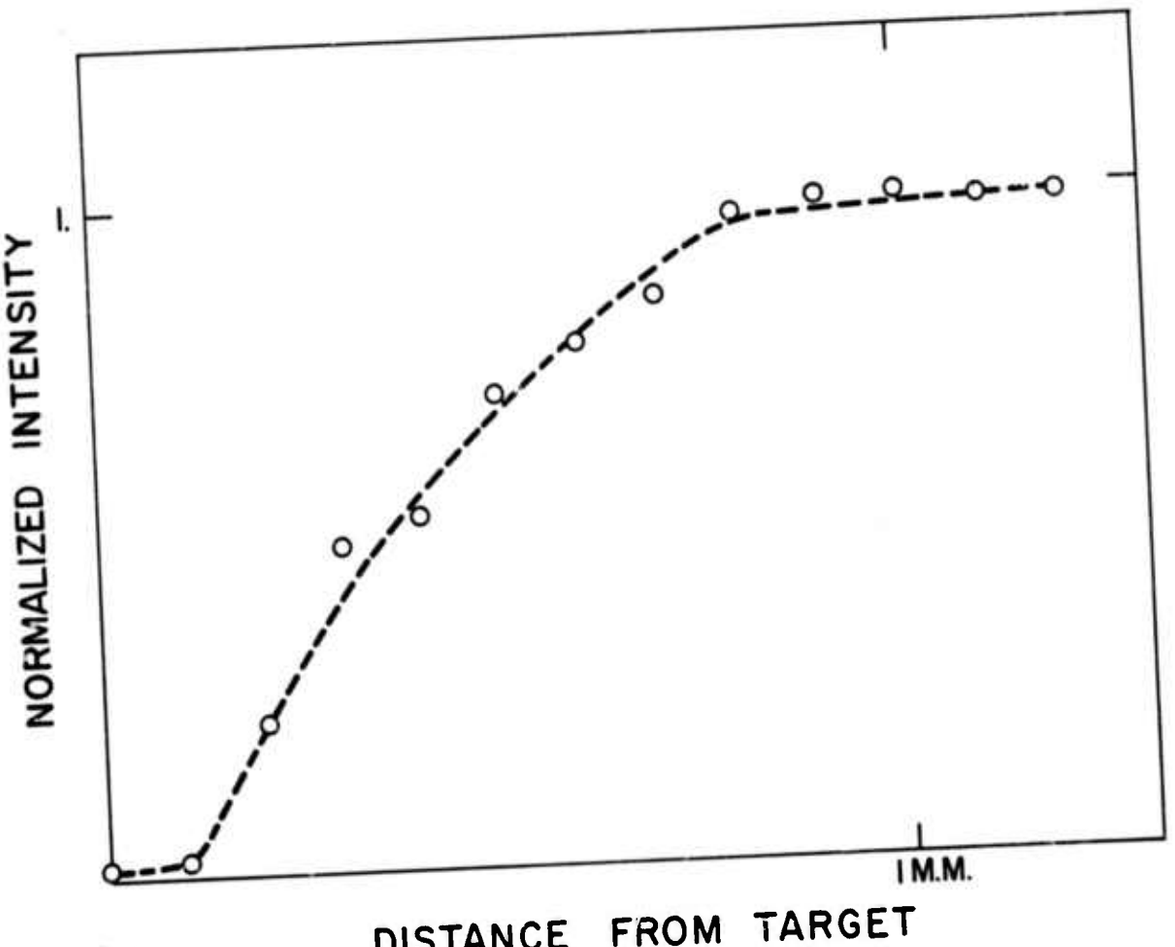

Fig. 3 Transmitted Intensity as a Function of Blade Position in Atomic Absorption Spectroscopy Probe Beam

contain a noble gas, usually Ne or Ar, and the emitted radiation consists of lines from these gases as well as lines from low density vaporized cathode material.

The standard operating current for these lamps is on the order of 10 mA which is more than adequate for their usual application. However, it was found that the intensity of the emitted radiation was insufficient for giving acceptable signal-to-noise ratios when time resolution on the order of 1 μsec is demanded as is the case in this investigation. To correct this situation, the lamps were maintained at their normal 10 mA DC level and then pulsed to a 2 amp level for a 200 μsec interval which included the time of the laser target interaction.

The "Breakdown Laser", an E-beam sustainer CO_2 laser device, was used to irradiate samples of Zn, Ti and Al. The pulse length was 100 μsec with energies ranging up to 100 J and the diameter of the first Airy ring was 4 mm. The laser energy was adjusted for a given sample so as to be just below or just above the breakdown level. Fluxes exceeding the breakdown threshold by even 20% would cause breakdown in times too short (less than a few μsec) to resolve the onset of target vaporization before the atomic absorption apparatus was overwhelmed with breakdown light.

3. Experimental Results

Figure 4 shows typical results obtained with a Ti target at a flux just below breakdown. The radiation from a titanium hollow cathode lamp passes within 1 mm of the target surface. The presence of titanium vapor is signaled by the onset of absorption of the 3643 Å radiation within $\approx$ 8 μsec of the laser turn on. As a control, radiation from a zinc hollow cathode lamp

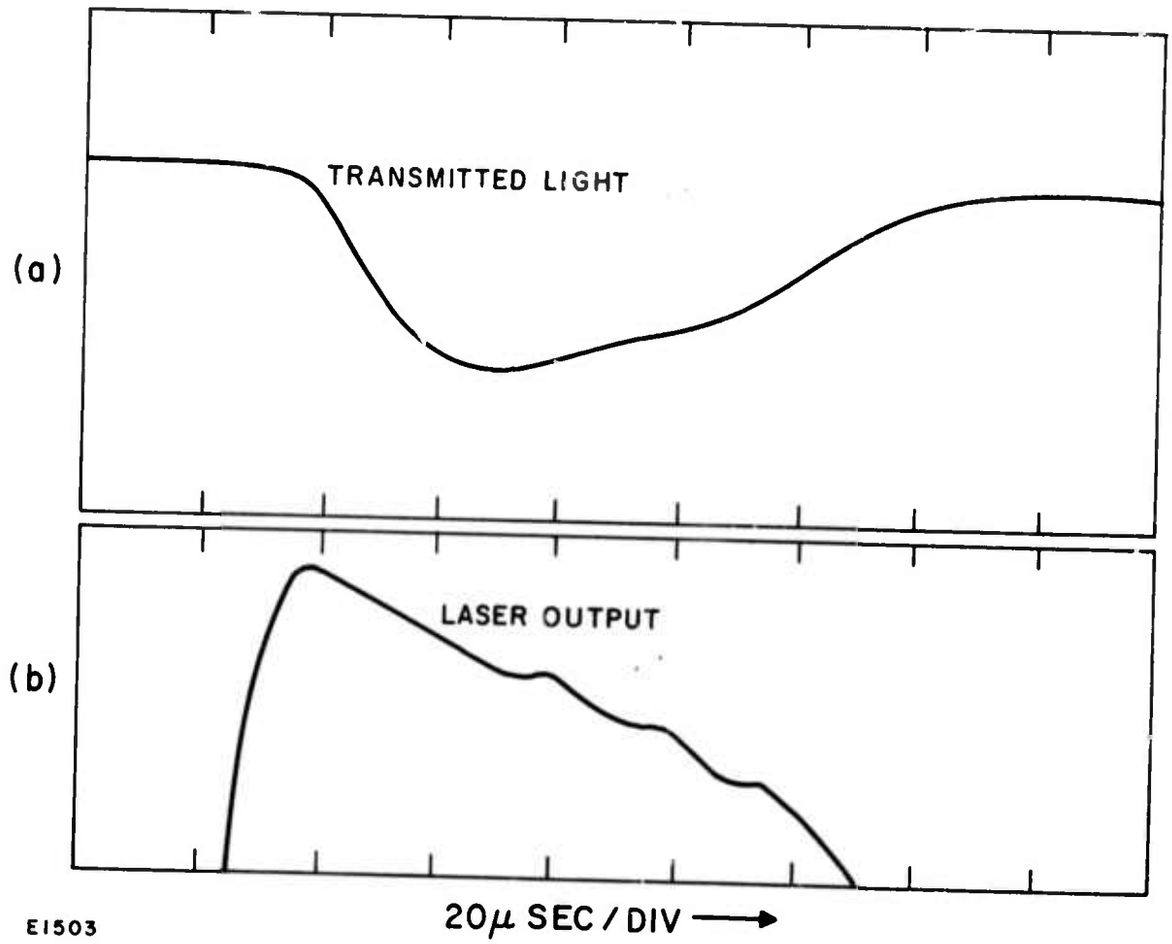

Fig. 4 (a) Transmission of 3643 Å Ti Light above a Ti Target
(b) Laser Output

was also passed above the target on subsequent shots (see Fig. 5). The fact that the nearby wavelength, 3076 Å, radiation is not affected shows that the decreases in signal observed with the Ti lamp are not due to distortions of the optical medium, but rather to resonance absorption by the Ti vapor. The experiments were also repeated with an Al lamp at 3093 Å (Fig. 6). Here even stronger absorption is observed and at an earlier time, $t \approx 4$ μsec, after laser turn on. The alloy employed was Ti 6, 4 consisting of 90% Ti, 6% Al and 4% vanadium. It appears that the aluminum constituent is distilling earlier from the sample due to its lower boiling point.

Experimental results for Al targets are presented in Fig. 7. The outputs from the gold doped germanium laser power monitor, the lower trace in each oscillogram, are unfiltered and show peaks of instantaneous intensity on the order of twice the average on-axis intensity of $\approx 7 \times 10^6$ watts/cm^2. The spikiness of the laser output is due to parasitic oscillations induced by feedback from the target. The top traces in each oscillogram show the transmission of the probe light and the zero transmission reference level. In oscillogram (a) absorption of resonant Al 3093 Å light appears within about 3 μsec of laser turn on. The absorption increases to approximately 60% at a time 30 μsec after laser turn on. The trace then disappears due to the large output of light associated with the plasma breakdown that occurs at that time.

After breakdown, the target spot appeared shiny against the as-received rolled surface. A following section will discuss the morphology of this melt zone in some detail. If the same spot was hit again with the laser, the results shown in oscillogram (b) were obtained. There was no

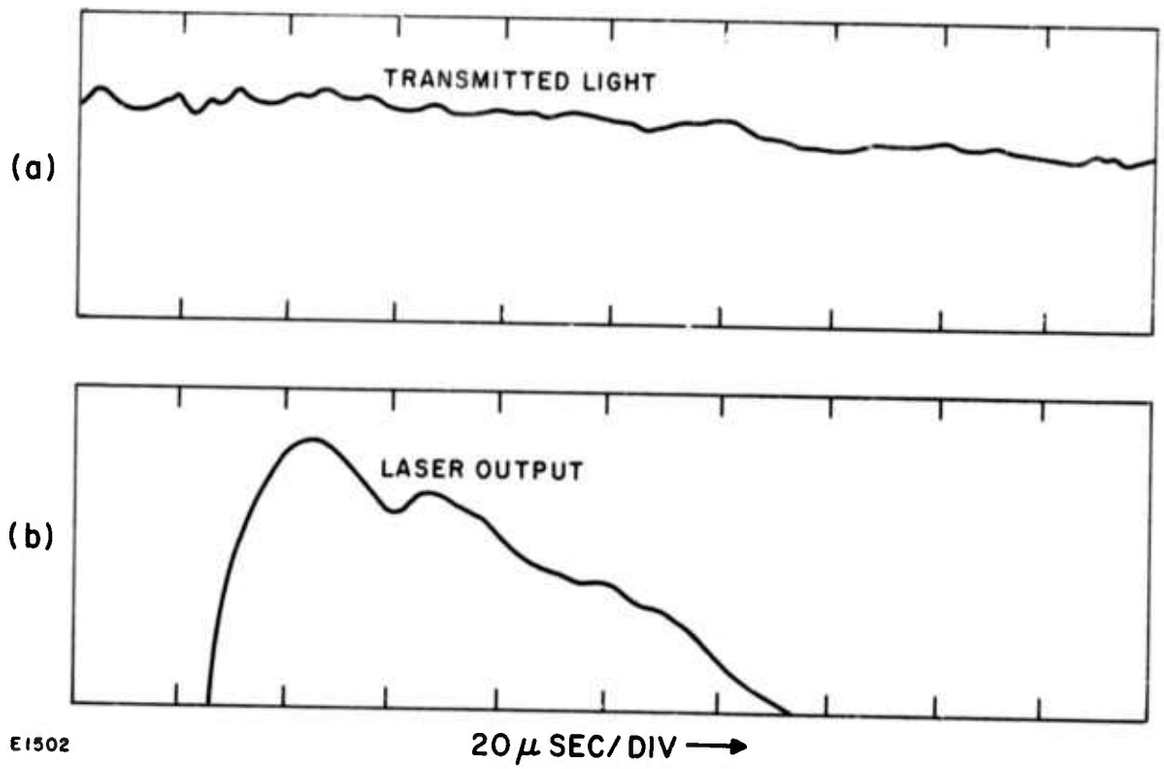

Fig. 5 (a) Transmission of 3076 Å Zn Light above a Ti Target
(b) Laser Output

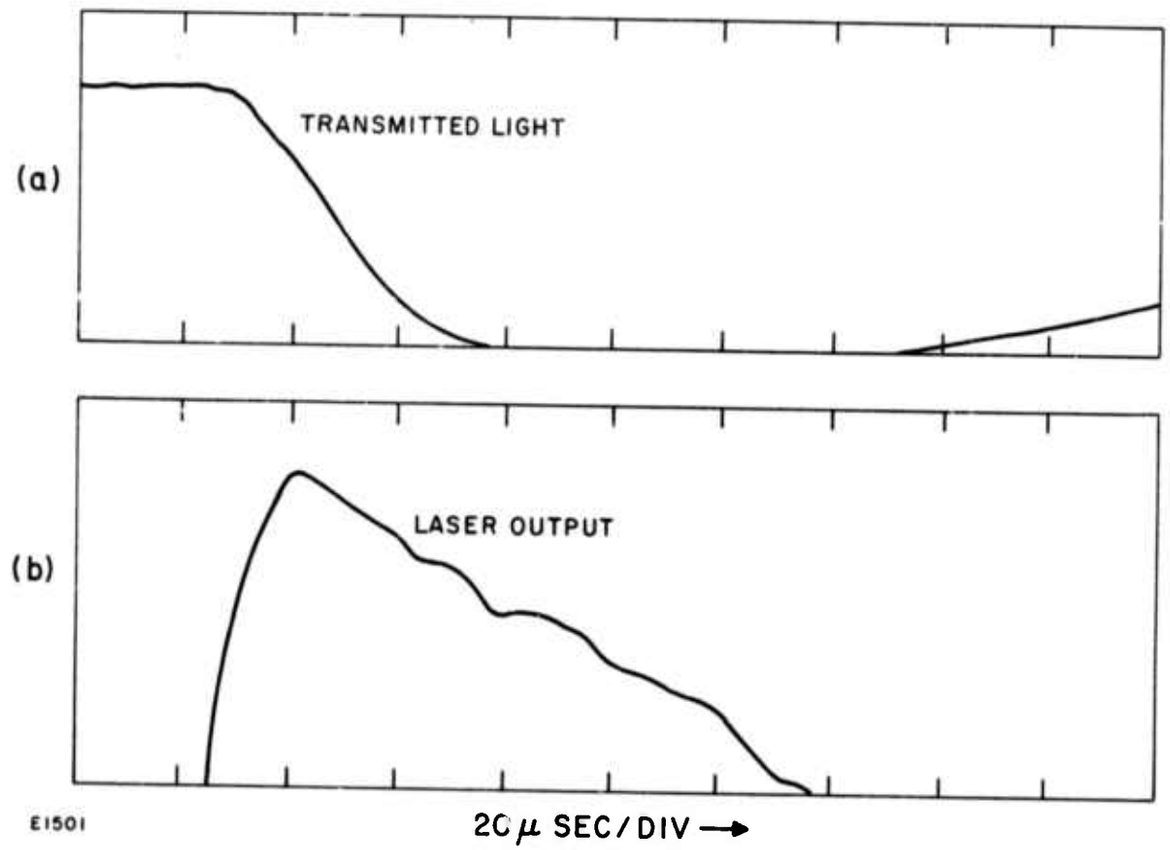

Fig. 6 (a) Transmission of 3093 Å Al Light above a Ti Target
(b) Laser Output

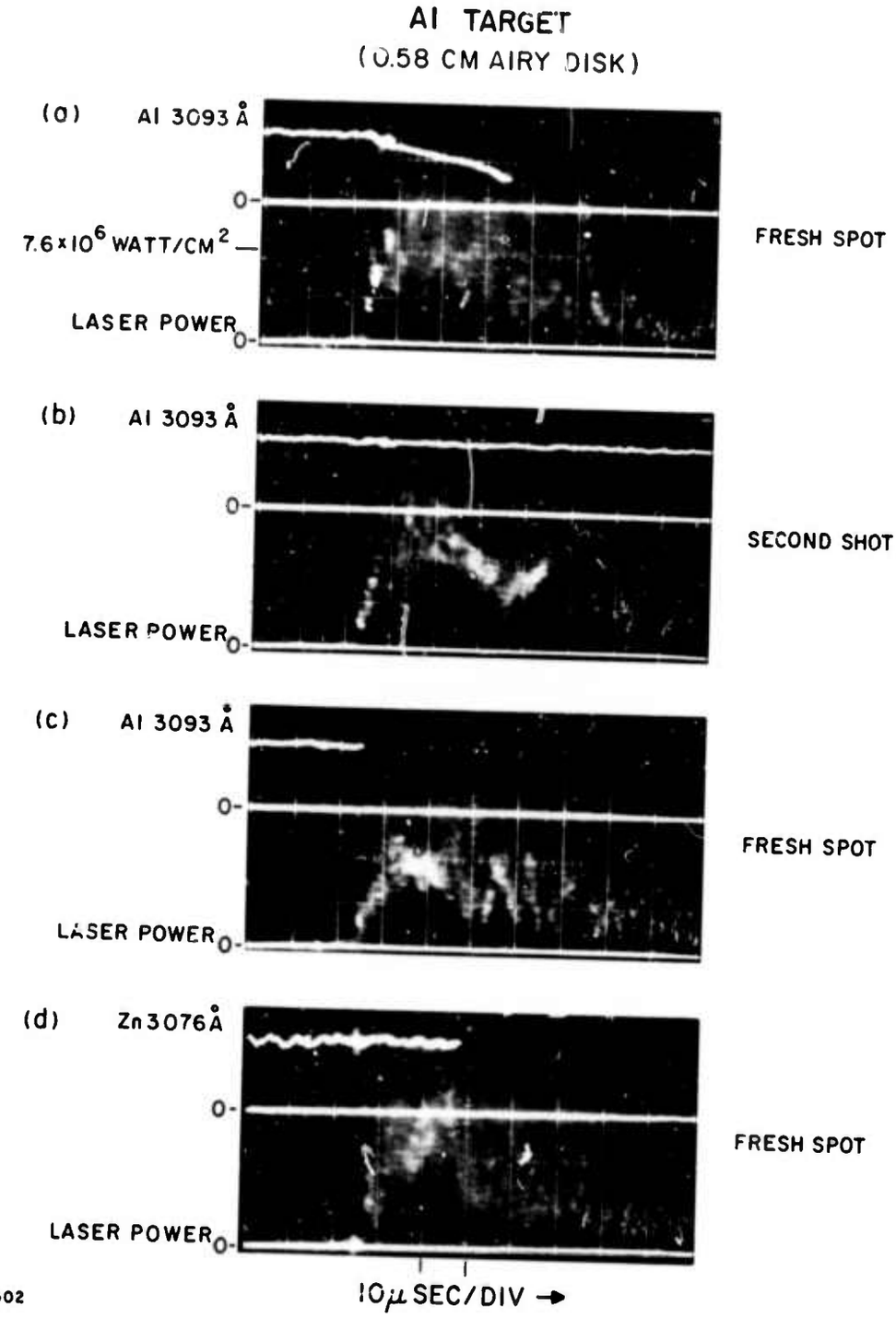

Fig. 7 Resonance Absorption Experiments on Al Targets. Top traces are transmitted probe light. Lower traces are laser power.

evidence of target vaporization and no plasma breakdown ensued. Subsequent shots would not ignite a breakdown even in the presence of intentionally introduced surface contamination in the form of fingerprints. However, a slight roughening of the surface with carborundum paper would ensure a breakdown on the following shot.

With laser power slightly above the threshold for breakdown, the time to breakdown varied randomly from a microsecond to tens of μsec. Absorption of Al resonant radiation was seen in all cases for which there was sufficient time for the vapor to block a significant portion of the probe beam and which were within the time response of the instrumentation. For those shots in which breakdown occurred within 2 μsec or less after laser turn on, such as shown in oscillogram (c), no direct evidence of vaporization was obtained. There is, however, no reason to assume that vapor was not present and that a new breakdown mechanism was operative in those cases.

Oscillogram (d) shows the transmission above the Al target of 3076 $\mathring{A}$ light from a Zn lamp. Here there is no absorption before the trace goes off scale at the time of breakdown, once again proving that true resonant absorption as opposed to refraction or scattering is being measured.

One case of particular interest was Zn, for which vapor was observed out to a distance of several cm in front of the target for times up to 1/2 sec after breakdown. Figure 8 shows the increase of the transmitted Zn lamp signal on a slow 100 msec/div time scale. The irregular nature of the increase was due to the random effects of the air currents that convected the vapor laden air out of the observation region. It should be noted that the Zn vapor was by this time quite cold and nonemitting. Indeed,

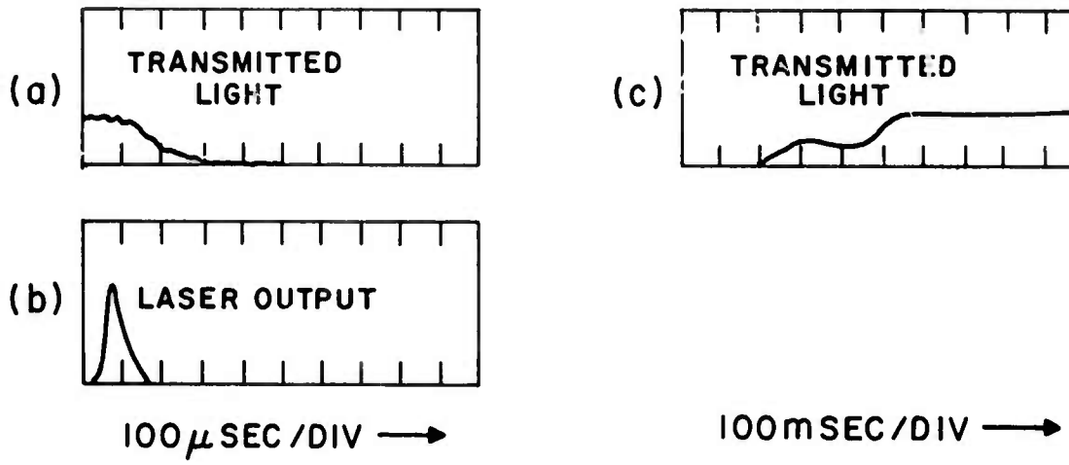

Fig. 8 (a, c) Transmission of 3076 Å Zn Light above a Zn Target
(b) Laser Output

interferograms of the breakdown, Fig. 9, show that the medium has returned to a relatively undisturbed condition by 10 msec after the laser pulse. These results suggest that caution should be used in interpreting multiple pulse experiments in which the air in front of the target is not changed between shots. Low levels of vapor undetectable by other means, could linger in the target area and trigger breakdowns away from the target surface.

B. TIME RESOLVED EMISSION SPECTROSCOPY

Atomic absorption spectroscopy provides a sensitive probe for the detection of most metallic vapors. The method does have its limitations. As mentioned, it is difficult to "see" vapor that is near the target surface. Moreover, the number of sources of resonance radiation is limited and it is quite possible that a surface contaminant, which would be undetected in a given experiment, could be evolving from the target and contributing to the breakdown process. Emission spectroscopy covering a broad spectral range can be useful here, given sufficient sensitivity and time resolution. Unfortunately, it may be shown that ordinary photographic film does not have the sensitivity to record emission from spectral lines radiating at intensities corresponding to a black body at Al vaporization temperature if time resolution of μsecs are demanded and spectrometers of reasonable f numbers are assumed.

1. Experimental Method

In answer to these shortcomings, a spectroscopic facility was assembled in which a gateable Silicon Intensifier Tube (S.I.T. tube) Optical Multichannel Analyzer (O.M.A.) manufactured by SSR Instrument Co. was used to record time resolved spectra. In essence, a visible spectrogram

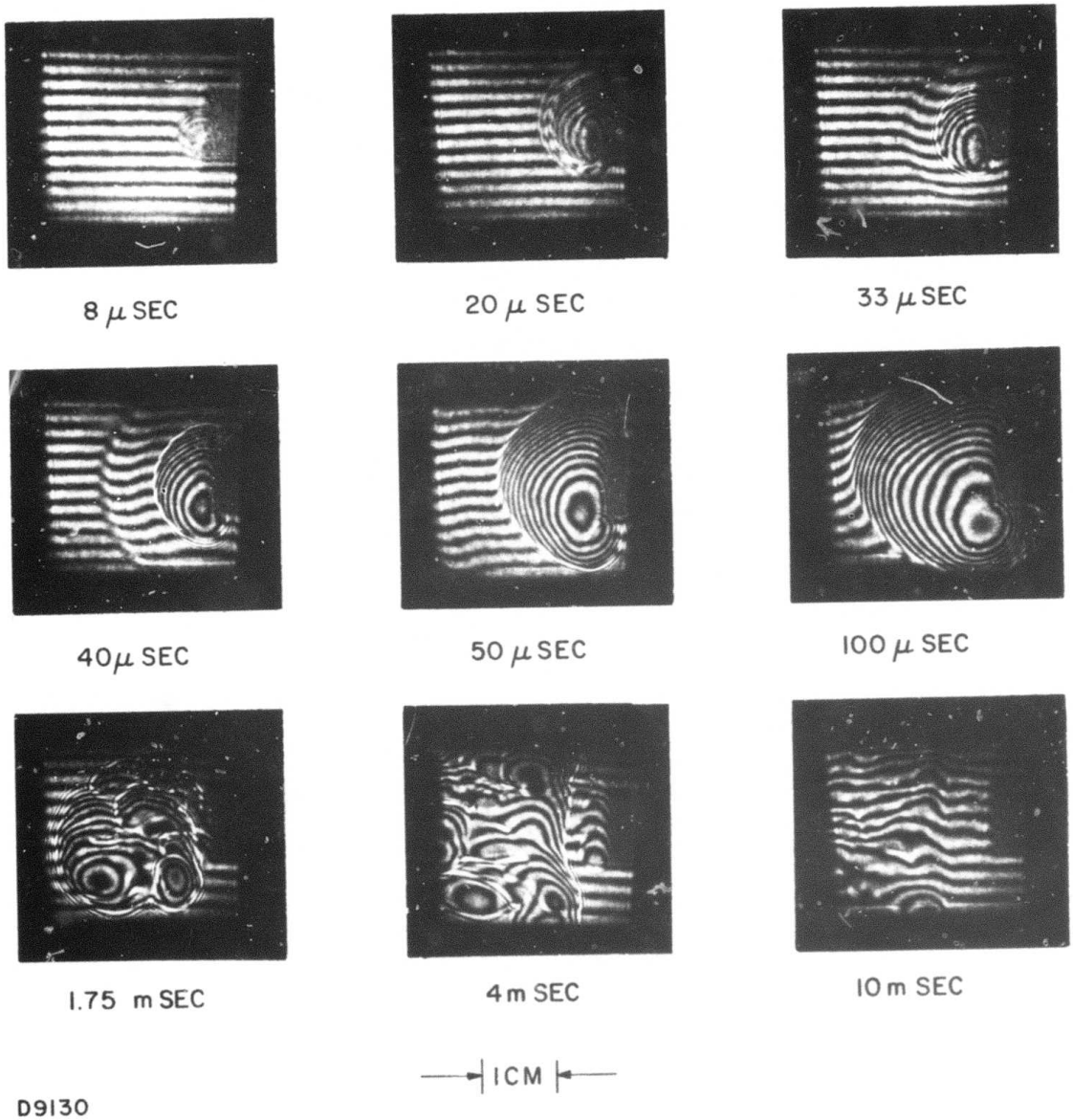

Fig. 9 Breakdown on an Unpolished Zinc Target

from a grating spectrograph is projected on the face of the S.I.T. photocathode. Photoelectrons from the cathode, whose passage is gateable to times as short as 100 nsec in synchronism with the experiment, are accelerated to a silicon target where a charge image is formed at a gain of 2000. This one-dimensional charge image is then read by a cathode ray beam and the resulting information is stored digitally in a 500 element memory bank. The data may be read out at any time to plot a complete spectrogram, or the individual spectral lines may be displayed and the area under them integrated.

A Jarrell Ash 1/4 meter monochromator with a 300 line per mm grating was modified for mounting the S.I.T. tube at the slitless exit plane. This provided a 1500 Å spectral coverage at 3 Å per channel with the central wavelength variable over the tube response range (S20 photocathode) by a grating rotation.

Successful application of the device demanded elimination of several sources of interference. Electrical pickup was avoided by slaving the laser to fire at a particular time with respect to the internal clock cycle of the O.M.A. unit. The S.I.T. tube proved to be quite sensitive to microphonics. This was a severe problem since shock waves resulting from a laser produced plasma breakdown disturbed the tube during the time that the silicon charge storage element was being read out by the electron beam. Gross noise in the spectra was finally removed by mounting the spectrometer tube assembly in a lead box lined with foam. The lens used to focus the target on the entrance slit served as a window for the box. These precautions provided the requisite acoustical damping.

Absolute intensity calibration of the unit was obtained by placing a standard tungsten lamp such that its filament occupied the position in the optical train that would normally be occupied by the laser target. Calibration was performed with the S. I. T. tube gated on for the same times as were used for recording plasma breakdown spectra. An electro-mechanical shutter of 20 ms open duration was placed between the filament and entrance slit to eliminate effects of imperfect blockage of light when the S. I. T. tube was in its off state.

2. Experimental Results

Spectral emissions from carbon targets were observed at an angle of 45° from the target normal. The gate pulse to the S. I. T. tube was set at 1 μsec width and the delay between the initiation of the laser pulse and the S. I. T. gate was varied between zero and one hundred μsec. The targets were irradiated at a central average flux level of 5×10^{6} watts/cm^{2}.

Figure 10 shows the resulting spectrum between 3500 Å and 5000 Å with a 1 μsec delay between laser and gate. A black body spectrum, with emissivity and temperature as free parameters, was fitted to the data at 7 points using the least mean square technique. This yielded a temperature of $3707^{\circ}K \pm 3\%$ and an emissivity of $0.70 \pm 30\%$. The Chi squared test showed a reasonable fit. The data was also fitted in the least mean square sense with only temperature as the free parameter and with emissivity held at the handbook value of 0.97. This gave a temperature of $3580^{\circ}K \pm 3\%$. Along with the experimental spectrum, Fig. 10 shows a $3580^{\circ}K$ spectrum that has been folded with the measured absolute spectral sensitivity of the spectrometer. It is evident that the observed spectrum can be attributed to a hot black body and that there are essentially no lines due to superheated impurities.

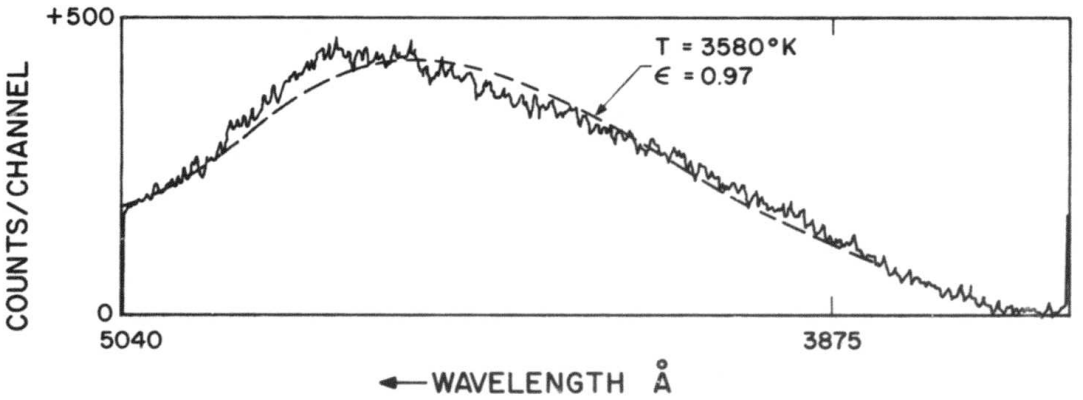

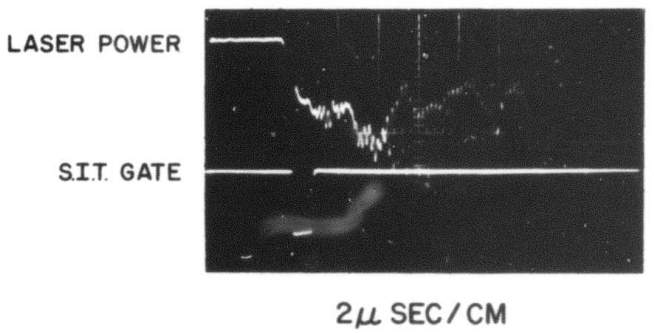

Fig. 10 Carbon Spectrum. Dashed line is a best fit 3580°K black body spectrum. Relative timing of laser and spectrum acquisition is shown in lower oscillogram

Similar results were obtained for a delay of 4 μsec between the start of the laser pulse and the start of the S.I.T. gate pulse. The temperature had increased to 4066°K $\pm$ 3% assuming 0.97 emissivity. As the delay was increased further to 7 μsec, the emission increased, but it was no longer possible to make a significant fit to the data with a black body curve. It appeared that the emissivity towards the red end of the spectrum was low compared to the emissivity at the blue end, a feature that persisted at longer delays.

Interferograms and shadowgrams were made of the carbon target to show its vaporization history (Fig. 11). A 300 nsec Xe pulsed laser at 5353 Å was used for illumination. The pictures were made on a shot-to-shot basis on fresh target spots, but reproducibility was good. It is evident that, for the longer delays, the spectrometer is viewing the target surface through a layer of blow-off vapor. If the vapor and the target have different temperatures and the optical depth of the vapor is less than unity and varies through the observed spectral regime, non-black body profiles would be expected. A useful extension of the present data would include observations of vapor alone by sighting the spectrometer at right angles to the target.

Preliminary emission spectra have also been obtained with Al targets. Figure 12 shows the emission in the wavelength range 3500 Å to 5000 Å. The spectrometer was oriented to view the target at an angle of 45° as with the carbon targets. For Fig. 12 the S.I.T. gate opened coincidentally with the start of the laser pulse and it remained open for 10 μsec. The laser flux was adjusted to a level just below the breakdown threshold.

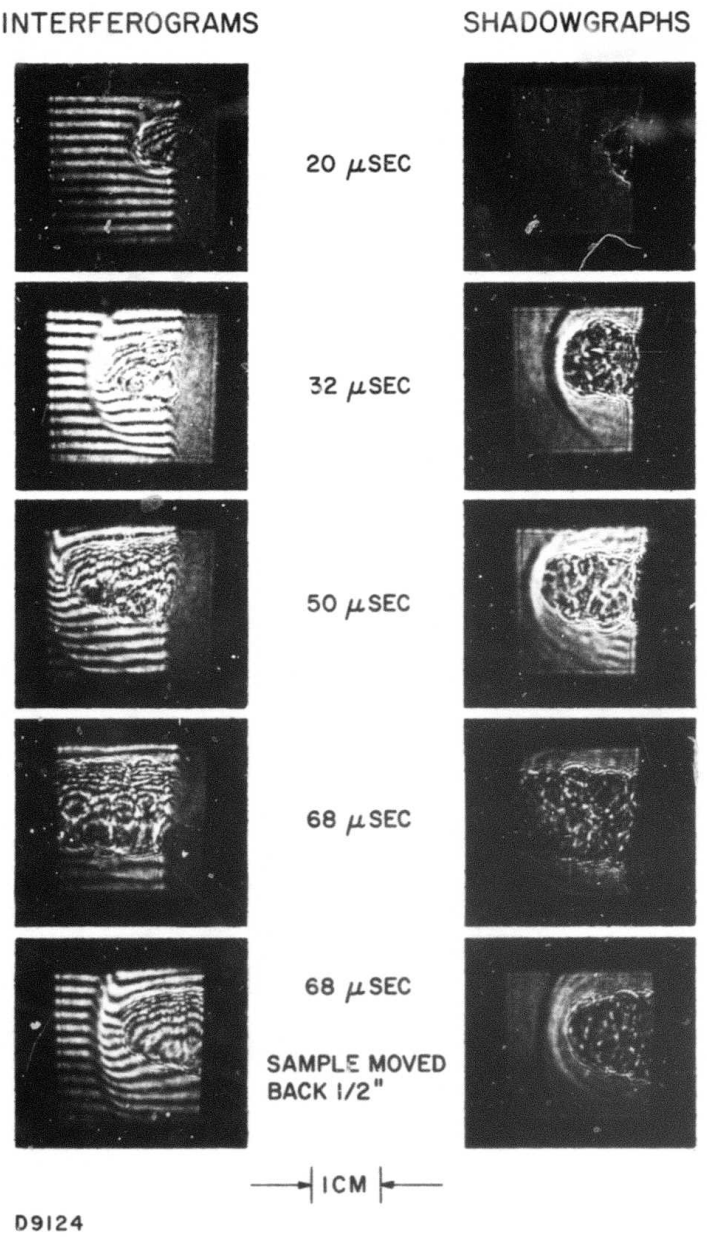

Fig. 11 Carbon Vapor Blowoff. Xe laser used for illumination.

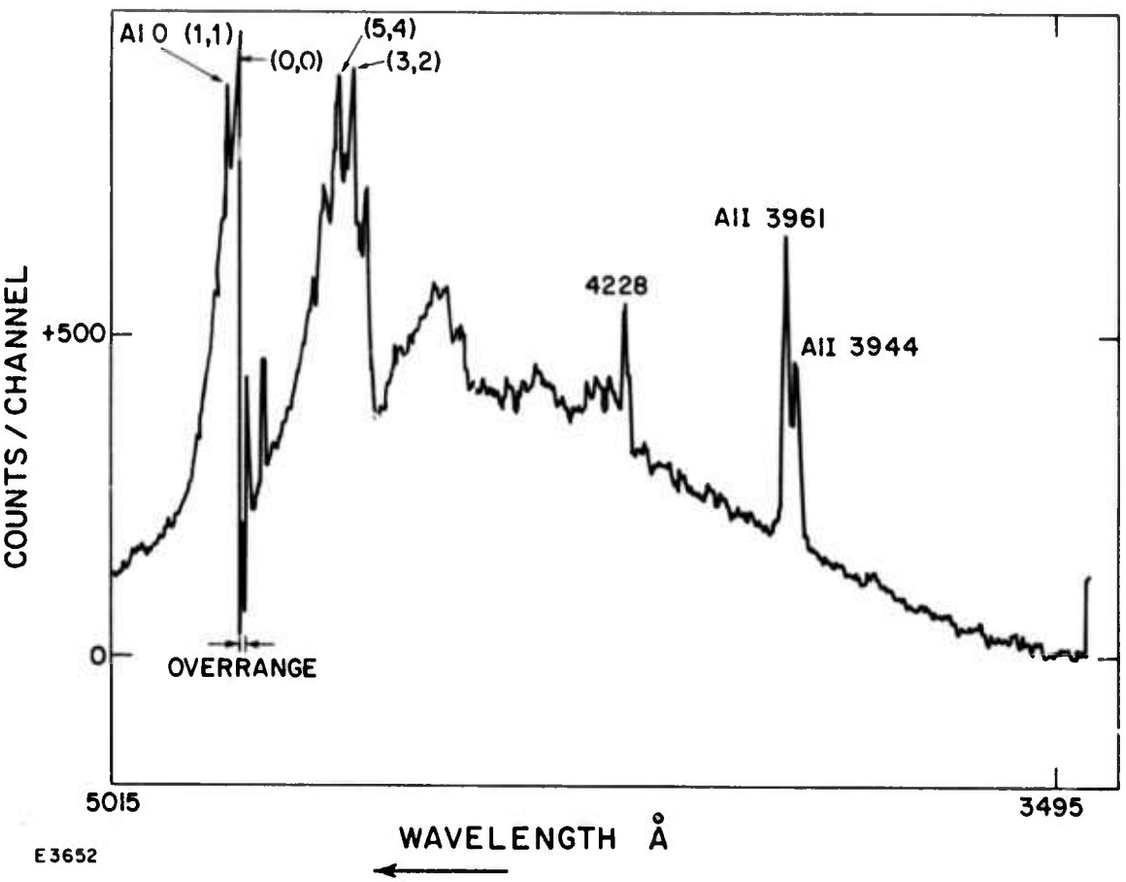

Fig. 12 Al Target Emission Spectrum during First 10 μsec of Laser Irradiation

Several atomic line and molecular band features appear superimposed on a broad continuum. In particular, the neutral Al lines at 3961 Å and 3944 Å are quite prominent. The molecular band system is due to AlO. At this point it is not clear whether the AlO is due to oxidation of Al vapor, or decomposition of a surface layer of hydroxide AlO (OH) or oxide Al_2O_3.

Some shots showed the as yet unidentified line at ≈ 4228 Å as the only prominent feature. Candidates are singly ionized aluminum at 4228 Å neutral copper at 4231 Å and neutral nitrogen at 4230 Å. Identification is complicated by the fact that wavelength uncertainty is ± 3 Å at the low dispersion employed. Copper is a 4.5% by weight constituent of the 2024 alloy used in this investigation. The boiling point of copper, 2868°C, is higher than Al, 2740°C, so it would be surprising if this material left the surface preferentially.

C. DISCUSSION

There are two principal questions regarding the data that has been presented. The first question deals with the time to reach vaporization temperature at a given flux and the second asks whether a plasma breakdown is to be expected in the observed times given the presence of vapor.

The time, τ, required for the surface of a uniform half space of material to increase in temperature by ΔT given a heat input to the surface of αI is

$$\tau = \frac{\pi}{4} \chi \left[\frac{\rho(c_p \Delta T + H)}{\alpha I} \right]^2$$

where χ is the thermal diffusivity, ρ is the mass density, c_p is the specific heat per unit mass, H is the heat per unit mass due to any phase change, I is the incident power per unit area and α is the energy absorptivity of the surface.

Given relatively high absorptivities at 10.6 μ, relatively low diffusivities and low vaporization temperature in the case of zinc, the theoretical vaporization times are shorter than the resolution time of the apparatus. Thus, the observation of prompt vaporization is not inconsistent with the model for these materials. Similarly, a carbon surface is predicted to reach the observed temperature of 3580°K in a time of $1.1 \times 10^6/(\alpha I)^2$ sec using a diffusivity of 9.3×10^{-2} cm^2/sec, heat capacity of 0.69 joules/°K-gm and a density of 1.73 gm/cm^3. The flux was 5×10^6 watts/cm^2 and the absorptivity is expected to be on the order of 50% leading to a predicted time of less than 1 μsec. Sublimation of the surface, which cannot be neglected at this temperature, would tend to thermostat the surface temperature.

In the case of aluminum targets, there is a large discrepancy between the observed vaporization time of 3 μsec or less at an average incident flux of $\approx 8 \times 10^6$ watts/cm^2 and the theoretical prediction of 520 μsec. This latter value is obtained under the assumptions of 3% absorptivity, a diffusivity of 0.35 cm^2/sec, and an energy per unit volume to reach vaporization, $\rho(c_p \Delta T + H)$, of 10.3 kJ/cm^3.

A plausible explanation for the fast vaporization can be based on the assumption of surface imperfections. Consider a surface that has detached flakes or a rough surface such as shown schematically in Fig. 13. It is assumed that the scale size of the imperfections, δ, is less than the thermal diffusion distance, $\sqrt{\chi t}$, where t is the time for the surface irregularity to reach vaporization temperature. By equating the absorbed energy per unit area of the imperfection divided by the dimension of the imperfection to the

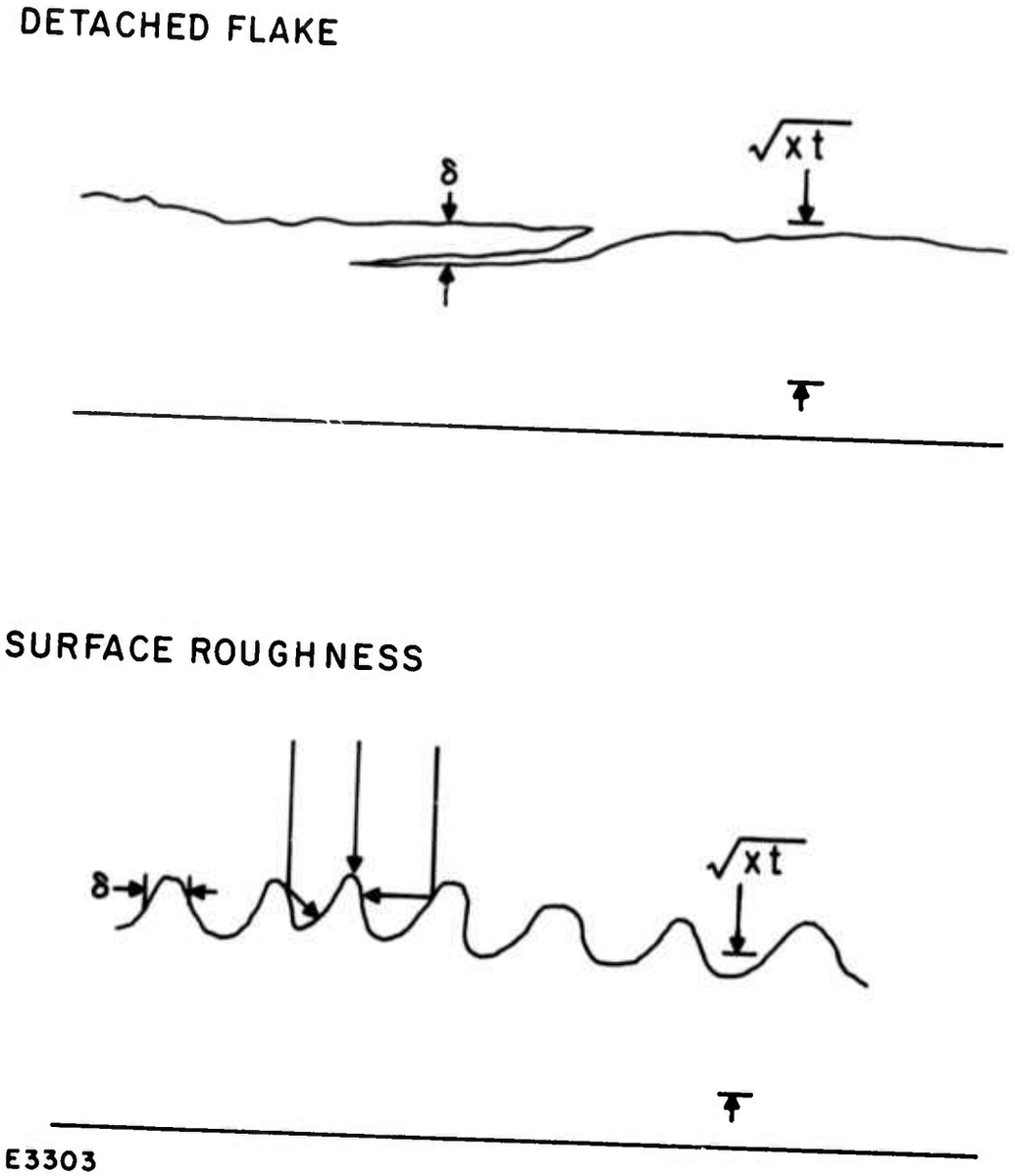

Fig. 13 Idealized Surface Imperfections. Heat diffusion is inhibited by crack in the upper drawing. Reflected laser radiation decreases temperature gradient and hence heat diffusion from point in lower drawing.

energy per unit volume necessary to reach vaporization temperature, a rough criterion for the vaporization time is obtained

$$t \approx \frac{\rho(c_p \Delta T + H)\,\delta}{\alpha I}$$

Alternately, this expression may be solved for the dimension δ given an observed vaporization time, t.

Using the observation that the aluminum targets were vaporizing in 3 μsec or less at 8×10^6 watts/cm^2, the inference is that imperfections of dimension less than on micron were responsible. This dimension is less than the approximately 10 μ diffusion depth at 3 μsec, consistent with our original assumption.

The evidence for surface imperfections is multifold. Time integrated and time resolved photographs show a number of localized bright spots on the surface during irradiation. Scanning electron micrographs of Al surfaces,[9] have revealed surface features that resemble the assumed flakes. Moreover, after irradiation with a CO_2 laser these micrographs indicate oxidation of the flakes as evidenced by their whiter appearance which would result from enhanced reflection of the scanning electrons by a nonconducting feature. Finally, there is the observation made in this report that vaporization did not occur when the surface had been melted by a previous laser shot. Such melting would, of course, tend to remove the micro-imperfections.

The time to heat Al vapor to full ionization as a function of incident 10.6 μ flux has been calculated by Thomas and Musal,[10] and by Boni, Cohen and Su.[6] Both calculations attribute electron heating to electron neutral inverse bremsstrahlung at low electron density and electron ion inverse bremsstrahlung at high electron density. Electrons lose energy through

ionization and elastic collisions with heavies. There are differences between the calculations. Thomas and Musal assume that ionization must take place between the ground state and the continuum, while Boni et al., argue that ionization proceeds through transitions to the first resonance level. For constant absorbed laser flux these assumptions lead to different electron temperatures but not radically different breakdown times. The reason is that absorbed laser power is approximately balanced by power going into ionization so the electron temperature will rise to whatever value is necessary to give the requisite ionization rate. (At fluxes much below 10^7 watts/cm^2 the calculations also differ due to their treatment of elastic cooling losses.)

For aluminum vapor leaving the target surface under conditions of temperature and pressure corresponding to steady-state vaporization with an incident flux of 10^7 watts/cm^2, Thomas and Musal predict breakdown (i.e., full ionization) in 0.1 μsec. More realistically they also compute a breakdown with initial conditions of 1 atmosphere pressure and the vapor at the Al boiling temperature (~2750°K). If the vapor is coming from small defect points on the surface as opposed to uniform planar vaporization, the pressure of the vapor would be expected to rapidly relax to 1 atmosphere. The predicted breakdown times by Thomas et al. and Boni et al., fall in the range of ten to fifty microseconds at a flux of 10^7 watts/cm^2. These compare favorably with many of the observed breakdown times. However, some breakdowns occurred in shorter times. One possible explanation would be the initiation of vaporization at more sites which would lead to a situation corresponding more to the steady-state initial conditions which are calculated to have shorter breakdown times.

III. ENHANCED TARGET DAMAGE

For most of the studies involving onset of target vaporization, the laser flux was adjusted to be on the borderline of the threshold for breakdown. The surfaces showed evidence of melt, the extent of which increased with laser power. Wherever the laser power was increased substantially above the breakdown threshold, on the order of 10% or more, gross cratering of the surface was observed. Figure 14 shows the change in surface appearance of 2024 T4 Al target samples as the laser flux is increased. Each photograph shows the effect of a single laser pulse. Breakdown was observed on all but the lower right sample. It is evident that the degree of cratering increases with laser flux.

A. DESCRIPTION OF EXPERIMENT

The samples were all taken from the same sheet of Al with the surface finish in an "as received" condition. Before irradiation the surfaces were cleaned with acetone followed by methyl alcohol.

Open shutter photographs were taken to show the extent of the breakdown plume and a photodiode was trained on the target to record the time history of light from the breakdown.

After irradiation the samples were accurately cross sectioned along the line forming the diameter of the damage spot. Employing standard metallurgraphic techniques, the samples were mounted in bakelite and the cross sectioned surfaces were polished and etched, Fig. 15. With a measuring microscope the depth of removed material on axis, and the depth of remaining melted material on axis were recorded, Table I.

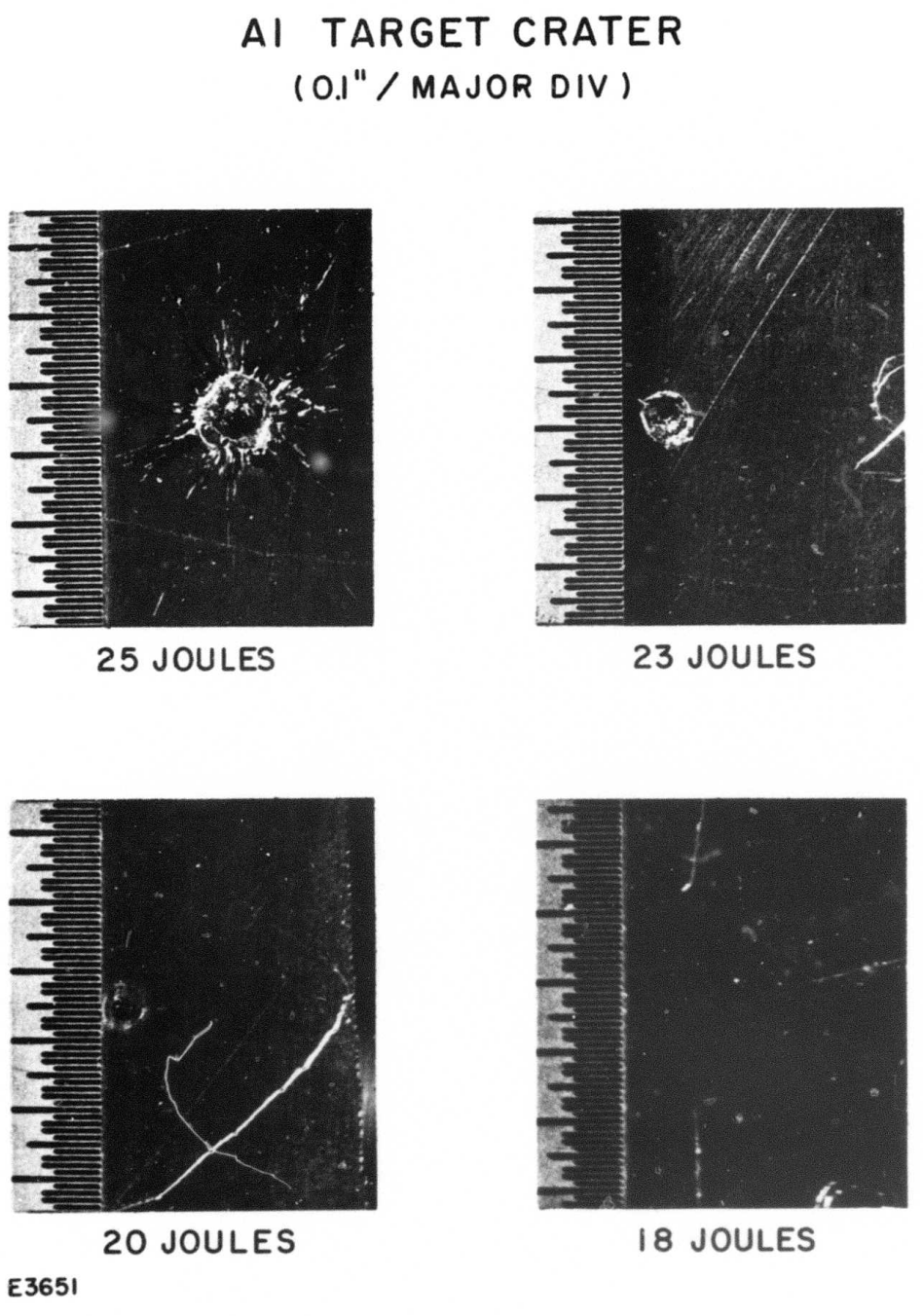

Fig. 14 Cratering on Al Targets as a Function of Incident Energy. Surface plasma breakdown occurred on all but the 18 joule shot.

ENHANCED COUPLING

2024 T4 Al
100 μSEC PULSE
2.9 mm AIRY DISK

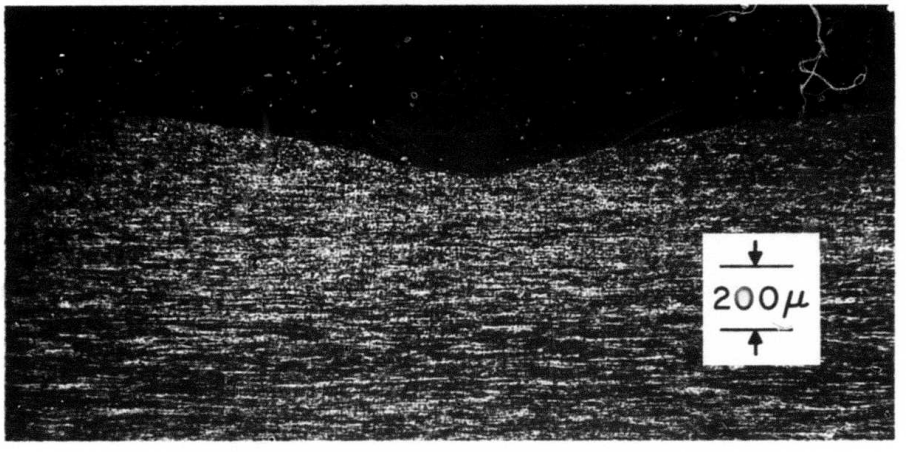

25 JOULES
SURFACE BREAKDOWN

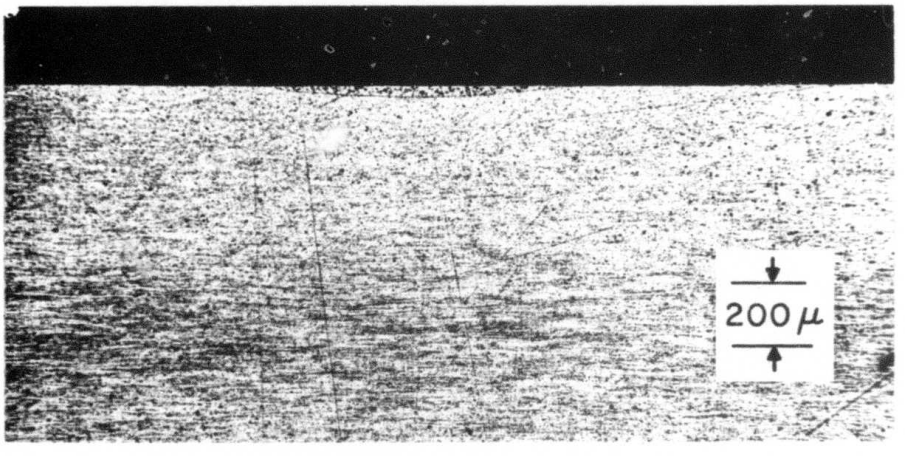

18 JOULES
NO BREAKDOWN

E1311

Fig. 15 Etched Cross Sections of Laser Damaged Al Targets

TABLE I

TARGET MELT REMOVAL AND THERMAL EFFECTS

Energy J	Axial Fluence J/cm^2	Melt Removal μ	Remaining Melt μ	Melt Fluence J/cm^2	Thermal Penetration μ	Thermal Fluence J/cm^2	Effective Coupling %
25	800	190	10	60	25	4	7.8
23	740	120	10	40	35	6	6.0
20	640	80	30	30	41	7	5.8
18	580	0	40	10	61	11	3.6

Relative instantaneous laser power was monitored with a gold doped germanium photodiode and the time integrated photodiode signal was standardized against total energy output as measured with a calorimeter. The theoretical value for the fluence, F_T, (energy per unit area) on axis at the focal point given a circular annular aperture with output coupling C is

$$F_T = (2.44)^2 \frac{\Pi}{4} \frac{C}{D_T^2} E_L$$

where D_T is the diameter of the first Airy disk at the focus and E_L is the total laser output energy. D_T was calculated from the optical system focal length and measured from lucite burn patterns as 0.29 cm. The output coupling, as defined by the geometry of the Breakdown Laser's unstable resonator was 0.80. The axial fluences employed in the data reduction to be presented were reduced by a factor of 0.72 from ideal based on previous (Ref. 11) detailed measurements in which the far-field intensity distribution was mapped by moving a narrow slit across the focal points.

B. ANALYSIS OF THERMAL COUPLING

An effective axial thermal coupling coefficient may be defined by the ratio

$$a = \frac{\rho Q_m (h_r + h_m) + \rho L_s h_s}{F}$$

where ρ is the density, 2.7 gm/cm^3, Q_m is the energy per unit mass to bring the material up to and including the molten state (1.05 kJ/gm) and L_s is the energy to bring the solid up to but not including the melt

temperature (651 J/gm). The depth of removed material is h_r, the depth of remaining solidified melt is h_m, and an effective thermal penetration depth is given as h_s. The total energy per unit area incident on the axis of the target is given by F.

The thermal penetration distance is obtained from the temperature distribution, T(z), in the solid phase

$$h_s \equiv \frac{1}{T_m - T_s} \int_0^\infty dz \, [T(z) - T_s]$$

where T_m is the melt temperature, T_s is the ambient temperature deep in the solid and z is a coordinate extending from the melt-solid boundary into the solid. During the laser pulse, the melt boundary is penetrating into the solid at velocity v which is assumed to be a constant equal to the final penetration distance divided by the laser pulse time, τ_p

$$v = \frac{h_r + h_m}{\tau_p}$$

An equation for the temperature distribution is most easily written by considering the thermal diffusion equation in a system of coordinates in which the melt-solid-boundary is stationary.

$$\frac{\partial T}{\partial t} - v \frac{\partial T}{\partial z} = \chi^2 \frac{\partial^2 T}{\partial z^2}$$

The diffusivity of the solid is taken as a constant (0.5 cm^2/sec for Al). This equation has the solution satisfying boundary conditions $T(t=0, z) = T_s$, $T(t, z=0) = T_m$ $T(t, z \to \infty) = T_s$, Ref. 12.

$$\frac{T - T_s}{T_m - T_s} = \frac{1}{2} \left[\operatorname{erfc} \frac{z+vt}{2\sqrt{\chi t}} + e^{\frac{-vz}{\chi}} \operatorname{erfc} \frac{z-vt}{2\sqrt{\chi t}} \right]$$

where erfc(x) is equal to one minus the error function, T_s is the temperature deep in the solid, and T_m is the melt temperature. The space integral between $z = 0$ and $z = \infty$ may be done with the help of relations given in Ref. 13.

$$h_s = \frac{\chi}{v} \operatorname{erf} \frac{v}{2\sqrt{\chi/t}} + (\chi t)^{1/2} i^1 \operatorname{erfc} \frac{v}{2\sqrt{\chi/t}}$$

In this expression, i^1 erfc(x) is the first integral of erfc(x) between the limits of x and infinity. This function is tabulated in Ref. 13. In the limit of vanishing velocity, series expansion of erf(x) gives

$$h_s \xrightarrow[v \to 0]{} \frac{2}{\sqrt{\pi}} (\chi t)^{1/2}$$

the well known result for thermal diffusion in a stationary medium. In the limit of velocity greater than the instantaneous thermal diffusion velocity

$$h_s \xrightarrow[v \gg \sqrt{\chi/t}]{} \frac{\chi}{v}$$

a result that may also be obtained by consideration of the steady-state problem with $\partial T/\partial t = 0$.

The computed values for h_s with $t = \tau_p$ are listed in Table I. It is noted that the thermal penetration depths are all significantly less than both the Airy disk diameter and the diameter of the melt affected zone. This justifies a one-dimensional approach to the diffusion problem.

From Table I it is seen that the effective axial coupling increased from 3.6%, a value that is not unreasonable for CW coupling, to 7.8% in the presence of a strong breakdown. Very little melt remained in the case of the strong breakdown

C. MELT REMOVAL

Some of the melt was undoubtedly removed in the form of droplets, since trails of burning droplets were observed in time exposed photographs and splash patterns radiated from the edge of the crater. Two actions could contribute to the melt removal. A radial pressure gradient is created in the liquid due to strong vaporization on the laser axis vs little or no vaporization as the radius of the first Airy disk is approached. The radial pressure gradient would accelerate the liquid tangent to the surface in a circularly symmetric pattern. A simple argument may be made to show that this effect is only to be expected at small spot sizes. From Bernouli's equation or from energy arguments, the average radial fluid velocity, U, will be approximately given by

$$\rho U^2 \approx P$$

where P is the on axis pressure. For Al vaporizing at a flux near 10^7 watts/cm^2 P may be shown to be of the order of 10 atm (10^7 dyne/cm^2). In order for the fluid to accelerate out of the crater within a pulse time, the velocity must satisfy

$$U > r/\tau_p$$

where r is the laser spot size. Thus

$$r \lesssim \tau_p \sqrt{P/\rho}$$

For a laser pulse of 100 μsec this implies that r must be less than a few millimeters. Since the spot diameter employed was approximately 3 mm diameter this mechanism is not inconsistent with observations.

A second mechanism, which is not limited to small spots, could also explain the observed cratering. Associated with the overpressure at the target surface due to vapor blowoff and plasma generation there is a radial outflow of vapor and heated air. This outflow is evident in the interferograms presented in Section I. Analysis of wave generation on the molten aluminum "sea" via the Kelvin-Helmholtz instability shows, Ref. 14, a half wavelength, $\lambda/2$, for maximum growth of

$$\frac{\lambda}{2} = \frac{3\pi\sigma}{2\rho'} \frac{1}{U'^2}$$

with an exponentiation time of

$$\tau_e = \left[\frac{270\sigma^2}{4\rho'^3}\right]^{1/2} \frac{1}{U'^3}$$

where σ is the molten metal surface tension (890 dyne/cm for Al) and U' is the velocity of the vapor of density ρ' tangent to the surface. For velocities near sonic in air (3.4×10^4 cm/sec) and hot high pressure gas (3000°K, 10 atm) with a density of 1.2×10^{-3} gm/cm^3, the half wavelength and growth time are respectively 26 μ and 2 μsec. Although these values indicate strong wave formation during the laser pulse time it should be noted that the theory totally neglects boundary layer effects which demand that the vapor velocity be zero at the surface and that our choice of vapor parameters, if not unreasonable, was at least somewhat cavalier. Clearly, a more complete instability theory is called for and better measurements or calculations of vapor flow properties above the surface are needed.

Once waves are formed on the surface, a simple argument may be made as to whether a droplet spray will be broken away from the wave peaks. Consider a protuberance on the surface with characteristic dimensions, D, both normal and parallel to the surface. The aerodynamic lift forces acting on the protuberence will be of the order $D^2\rho' U'^2$. When these forces are greater than the surface tension forces, of order σD, which hold the protuberence to the bulk of the melt, a free droplet will be formed. Thus, projections with dimensions satisfying

$$D > \frac{\sigma}{\rho' U'^2}$$

will form a spray. It is noted that this critical dimension is of the same order as the half wavelength for maximum growth of the Kelvin-Helmholtz instability. Thus, wave generated droplet spray remains an alternative for explaining the observed cratering. This mechanism should remain operative for large target spot sizes and could be enhanced by air flows on the order of Mach 1 over the target surface.

REFERENCES

1. Kroll, N., Watson, K., "Theoretical Study of Ionization of Air by Intense Laser Pulses," Phys. Rev. A, 5, 1883 (1972).

2. Smith, D., Investigation of Gas Breakdown With 10.6 Micron Wavelength Radiation, United Aircraft Research Laboratories Report, AFWL-TR-72-182 (Feb. 1973).

3. Gilbert, K.G., Carlson, R.L., A Comparative Experimental Study of Material Interactions for Repetitively Pulsed and Continuous Wave CO_2 Lasers, Air Force Weapons Laboratory Report, AFWL-TR-72-168 (Nov. 1972).

4. Pirri, A.N., Theory for Momentum Transfer to a Surface with a High Power Laser, Avco Everett Research Laboratory, AMP 350, Contract No. F-4701-72-C-0264 (March 1973).

5. Thomas, P.D., and Musal, A.M., A Theoretical Study of Laser-Target Interaction, Lockheed Missile and Space Co., Report LMSC-D352890 (Aug. 1973).

6. Boni, A.H., Cohen, H.D., and Su, F.Y., A Theoretical Description of the Interaction of an Intense Laser Beam with a Solid Target, Systems Science and Software Report SSS-R-73-1860 (Aug. 1973).

7. Elwell, W., and Gidley, J., Atomic-Absorption Spectrophotometry, 2nd Ed., Pergamon Press, Ltd., London 1966.

8. Griem, H.R., Plasma Spectroscopy, McGraw Hill, N.Y. p. 95 (1964).

9. Walters, C.T. and Barnes, R.H., An Investigation of Mechanisms of Initiation of Laser-Supported Absorption (LSA) Waves, Battelle Columbus Laboratories, Semi-Annual Report, Contract #DAAH01-73-C-0776 (Nov. 1973).

10. Thomas, P.D. and Musal, H.M., A Theoretical Study of Laser Target Interaction, Lockheed Missile and Space Co., Report LMSC-D313142 (Dec. 1972).

11. Schlier, R., Pirri, A., Reilly, D., "Air Breakdown Studies," Avco Corp. Report prepared for Air Force Weapons Laboratory, AFWL-TR-72-74, Contract No. F29601-70-C-0073 (Feb. 1973).

12. Carslaw, H. and Jaeger, J., Conduction of Heat in Solids, 2nd Ed., Clarendon, p. 388 (1959).

13. Abramowitz, M. and Stegun, I.A., Ed., Handbook of Mathematical Functions, National Bureau of Standards, AMS 55 (1964).

14. From notes by Johnson, R.L., O'Keefe, J.D., "Laser Burnthrough Time Reduction by Hydrodynamic Instability of the Melt Layer," TRW Systems Group.